Journal Pre-proof

Reliability enhancement of state of health assessment model of lithium-ion battery considering the uncertainty with quantile distribution of deep features

Ying Zhang, Ming Zhang, Chao Liu, Zhipeng Feng, Yuchun Xu

PII: S0951-8320(24)00077-2
DOI: https://doi.org/10.1016/j.ress.2024.110002
Reference: RESS 110002

To appear in: *Reliability Engineering and System Safety*

Please cite this article as: Y. Zhang, M. Zhang, C. Liu et al., Reliability enhancement of state of health assessment model of lithium-ion battery considering the uncertainty with quantile distribution of deep features. *Reliability Engineering and System Safety* (2024), doi: https://doi.org/10.1016/j.ress.2024.110002.

Reliability Enhancement of State of Health Assessment Model of Lithium-ion Battery Considering the Uncertainty with Quantile Distribution of Deep Features

Ying Zhang[a], Ming Zhang[b,*], Chao Liu[b], Zhipeng Feng[a], Yuchun Xu[b]

[a] *School of Mechanical Engineering, University of Science and Technology Beijing, Beijing, 100084, China*
[b] *College of Engineering and Physical Sciences, Aston University, B4 7ET Birmingham, U.K.*

Abstract

Lithium-ion batteries (LIBs) are widely used in many fields, such as electric vehicles and energy storage, and directly impact the device performance and safety. Therefore, the state of health (SOH) assessment is critical for LIB usage. However, most of the existing data-driven SOH modeling methods overlook the inherent uncertainty in battery health prediction, which decreases the reliability of the model. To address this issue, this paper proposes a novel SOH assessment model based on the deep learning framework. The SOH results are derived from the quantile distribution of deep features, giving the SOH values with associated confidence intervals. This enhances the reliability and generalization of SOH assessment results. Additionally, to complete the optimization of the deep model, a Wasserstein distance-based quantile Huber (QH) loss function is developed. This function integrates Huber loss and quantile regression loss, enabling the model to be optimized based on a distribution output. The proposed method is validated using the NASA dataset, and the results confirm that the proposed method can effectively estimate the SOH of LIB while accounting for uncertainty. The incorporation of SOH distribution enhances the reliability and generalization ability of the SOH assessment model.

Keywords: Model reliability; State of health; Lithium-ion battery; Wasserstein Distance; Uncertainty; Quantile Distribution

Abbreviation	Full Name	Abbreviation	Full Name
SOH	State of Health	LIB	Lithium-ion Battery
QH	Quantile Huber	EIS	Electrochemical Impedance Spectroscop
CNN	Convolutional Neural Network	ResNet	Residual Network
LSTM	Long Short-Term Memory	CDF	Cumulative Distribution Function
GPR	Gaussian Process Regression	CV	Constant Voltage
CC	Constant Current	MAE	Mean Absolute Error
RMSE	Root Mean Square Error		

1. Introduction

The state of health (SOH) assessment of lithium-ion batteries (LIBs) is crucial in various applications, such as electric vehicles and renewable energy storage [1]. The SOH of LIBs directly affects the operating performance of these devices [2]. The SOH assessment provides valuable information about the current condition of a battery. With the LIBs aging and degrading, the energy capacity and runtime reduce gradually over time [3]. They become more prone to safety issues, such as overheating, thermal runaway, and even fires or explosions [4].In this regard, SOH assessment allows users to monitor and optimize battery performance in time, which would help in identifying potential safety risks and preventing catastrophic failures.

*Corresponding author
Email: m.zhang21@aston.ac.uk

SOH assessment remains an active area of research and development [5]. The SOH of a LIB denotes its present health condition in relation to its nominal performance [6]. Typically, it involves calculating the ratio of the current-cycle capacity to the initial-cycle capacity [7]. Various methods such as charge/discharge tests [8] and Electrochemical Impedance Spectroscopy (EIS) [9, 10], can be used to assess the LIB SOH. These techniques provide insights into a battery's capacity, internal resistance, chemical aging and other factors that affect its health and performance, but it demands long rest times to avoid the effect of relaxation to the EIS measurement [11]. This impacts both data accessibility and model construction. With the advent of the Internet of Things (IoT), collecting data for SOH monitoring has become more convenient [12, 13]. Voltage, current, and temperature signals obtained from battery management systems during operation have surpassed EIS data in terms of monitoring capabilities, enabling real-time SOH assessment.

Voltage, current, and temperature signals are widely used for modeling SOH assessment. They can reflect the internal health state of LIB effectively [14]. Researchers have proposed models utilizing these signals for effective SOH prediction. For instance, Wen et al. devised a battery SOH prediction model based on incremental capacity analysis and a BP neural network [15]. This model established a correlation between temperature and incremental capacity curve characteristics to predict battery SOH values at various temperatures. Similarly, Cheng et al. proposed an optimal dispatch approach for online SOH estimation [16], accounting for degradation. This online SOH estimation model utilized the Kalman filter for estimation, achieving higher accuracy by integrating short-term estimation and long-term prediction results. Jia et al. proposed an indirect health indicators constructed from voltage, current, and temperature signals of charging and discharging. Then the short-term SOH prediction is conducted by combining the Gaussian process regression (GPR) method with probability predictions [17]. These research conducted SOH assessment of LIB based on the widely-used voltage, current and temperature data. The SOH results provide important suggestions for LIB maintenance. The application of these methods prolongs the lifespan of LIB and enhance the sustainability across various applications and industries. However, these methods rely heavily on the expertise and prior knowledge to extract the proper features, imposing significant limitations on their applicability.

Deep learning-based approaches for LIB SOH assessment have gained attention due to their success in self-adaptively modeling complex nonlinear systems [18, 19]. Su et al. proposed a hybrid method that fuses the battery equivalent circuit model and the convolutional neural network for battery health state monitoring [20]. Ma et al. developed a novel SOH estimation method by fusing multiple health indicators based on a hybrid network with deep belief network and long short-term memory (LSTM) [21]. Deep features were extracted effectively from the monitoring data. Wang et al. proposed a bioinspired spiking spatio-temporal attention framework for the LIB SOH. This work utilizes precise battery physical and chemical degradation information and brain-inspired spiking neural networks for accurate SOH estimation based on the full-life-cycle EIS data [22]. Though deep learning methods attain good performance in the application of LIB SOH assessment, these models tend to give a specific value of the SOH. These outcomes overlook the inherent uncertainty generated in the data collection and estimation process [23, 24]. The figure 1 is given as an example to facilitate the understanding of uncertainty that exists in LIB SOH monitoring data. The figure illustrates the partial variations in the charging current of batteries #5, #6, and #7 from the NASA dataset [25] at the 100th cycle. Theoretically, the current variation of the three batteries should be consistent. However, the figure reveals slight variations in current values, even at the same cycle. This discrepancy can be attributed to uncertainties during cycling, leading to unpredictable fluctuations in the estimated SOH.

Uncertainty refers to a lack of certainty or confidence in the outcome of a particular event or situation [26]. In the SOH assessment of, uncertainty encompasses two key components. First, aleatoric uncertainty. This type of uncertainty is often related with random events or stochastic processes generated during SOH monitoring data collection. Second, epistemic uncertainty. It represents the uncertainty that arises from the absence of SOH assessment knowledge, and it can potentially be reduced or eliminated with additional information, improved models, etc. [27]. Deep learning models, while achieving good performance, may not consider these uncertainties, leading to diminished generalization and reliability. Therefore, constructing a trustworthy and reliable model becomes crucial for SOH assessment of LIB, particularly in the context of deep learning. Efforts have been made to address this issue. Zhou et al. investigated the trustworthy model of fault diagnosis in a probabilistic Bayesian deep learning framework [28]. This method incorporated an uncertainty-aware model to translate the fault information and recognize the monitoring data from unseen domains. Though this work focused on uncertainty influence, it necessitated additional prior knowledge for uncertainty modeling. Wang et al. introduced an explainability-driven model improvement framework for

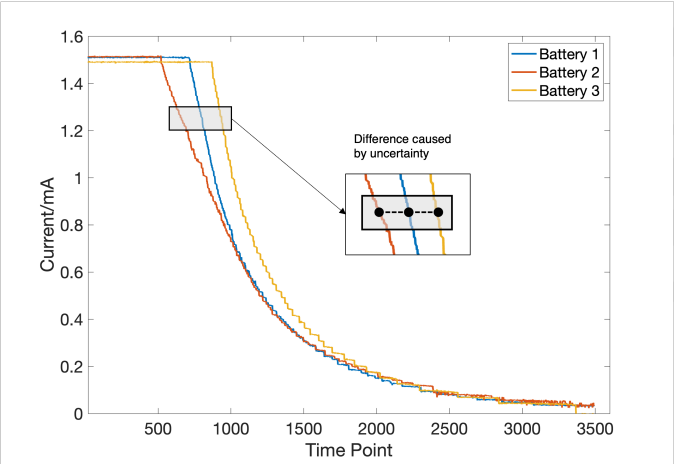

Figure 1: Current of three batteries at the cycle of 100

LIB SOH estimation [29]. This framework delves into further exploration of the explainability of the SOH model. However, this research does not address the output reliability of the SOH model. Tagasovska et al. presented single-model estimates of aleatoric and epistemic uncertainty for deep neural networks using simultaneous quantile regression [30]. This approach can map out-of-distribution examples to non-zero values, indicating epistemic uncertainty and contributing to the construction of a more trustworthy model. This work demonstrates the feasibility of constructing a distribution to enhance the trustworthiness of the model.

Inspired by the work on simultaneous quantile regression for uncertainty estimation in deep neural networks [30], this study proposes incorporating quantile regression for SOH distribution estimation. This approach provides a distribution of SOH values, considering the inherent uncertainties in the system and measurements during cycling. The output offers more reliable information for LIB maintenance, enhancing the precision and reliability of SOH estimation. This method contributes to the construction of a trustworthy model for LIB SOH assessment. It considers both aleatoric and epistemic uncertainties, thereby improving the precision and reliability of SOH estimation.

The main contributions are summarized as follows.

1. A novel SOH assessment framework based on deep learning is proposed. This framework includes the construction of SOH reference distribution, ResNet model training on multi-source data for deep feature extraction, model test and method evaluation and visualization. Multi-source data can capture comprehensive information for SOH.
2. A SOH assessment model that considers the uncertainty is proposed for of LIB. A quantile distribution of deep features is constructed to give a predicted distribution of SOH values with associated confidence interval. It enhances the reliability of SOH results and obtains a result of high generalization.
3. A Wasserstein distance-based QH loss function has been designed to calculate the inverse cumulative distribution function(CDF) divergence between estimation and reference of SOH. This loss function incorporates the Huber loss and the quantile regression loss. It demonstrates better performance than the traditional loss function of mean absolute error(MAE) and mean square error(MSE).

The rest of this paper is arranged as follows. Section 2 gives the theoretical preliminaries of the proposed method. Section 3 formulates the problem of SOH assessment. Section 4 introduces the construction of the SOH model Section 5 validates the proposed method using the NASA dataset and evaluates the performance of the proposed method. Section 6 gives the conclusion and discussion of the research.

2. Preliminary

This section provides the foundational knowledge essential for introducing our proposed methodology. Within our approach, the Wasserstein distance is used to optimize the traditional Huber loss and the quan-

tile loss. This optimization process enables the development of a network that yields the SOH distribution as its outcome. The quantile regression is also introduced. It is used in our methodology for SOH distribution prediction.

2.1. Wasserstein Distance

The Wasserstein distance, also known as the Earth Mover's distance or optimal transport distance, is a measure of the distance between two probability distributions over a region. It quantifies the minimum cost that is used to transform one distribution into the other. The distance metric proves especially beneficial in scenarios involving distributions with divergent masses or shapes. This function holds the continuous and differentiable property everywhere. It is the basis to derive the proposed loss function in this work.

The Wasserstein distance derivation involves advanced mathematical concepts from optimal transport theory. Given two probability measures U_1 and U_2 defined on a metric space $(\mathcal{X}, d)$, the p-Wasserstein distance is defined as

$$W_p(U_1, U_2) = \inf_{\gamma \in \Gamma(U_1, U_2)} f_{\mathcal{X}\times\mathcal{X}} d(x, y) d\gamma(x, y) \tag{1}$$

where $\Gamma(U_1, U_2)$ is the set of all joint distributions on $\mathcal{X} \times \mathcal{X}$ with marginals U_1 and U_2. d is the ground distance function representing the cost of transporting mass from x to y.

When U_1 and U_2 are two probability distributions with cumulative distribution functions, the p-Wasserstein metric W_p can be defined as [31]

$$W_p\left(U_1, U_2\right) = \left(\int_{-\infty}^{+\infty} \left| F_{U_1}^{-1}(\tau) - F_{U_2}^{-1}(\tau) \right| \mathbf{d}\tau \right)^{1/p} \tag{2}$$

where τ is the quantile. F^{-1} represents the quantile functions (inverse CDFs). It can be expressed as

$$F_U^{-1}(\tau) := \inf\{x \in \mathbb{R} : \tau \leqslant F_U(x)\} \tag{3}$$

where $F_U(x) = Pr(U \leqslant x)$ is the CDF of random variable U.

2.2. Quantile Regression

Quantile regression is a statistical technique used to model the conditional quantiles of a response variable. Unlike traditional regression methods that focus on estimating the conditional mean of the response variable, quantile regression allows for the modeling of different quantiles, providing a more comprehensive view of the conditional distribution.

Quantiles represent points in a distribution below which a certain proportion of the data falls. Common quantiles include the median (50th percentile), quartiles (25th and 75th percentiles), and other percentiles. The objective of quantile regression is to estimate the conditional quantiles of the response variable. For a given quantile τ, the objective function is defined as [32]

$$Q_\tau = \sum_{i=1}^{n} \rho_\tau(y_i - X_i\beta) \tag{4}$$

where Q_τ is the quantile loss function, y_i is the observed response for the i-th observation, X_i is the predictor matrix for the i-th observation, β is the vector of coefficients to be estimated, and $\rho_\tau(u)$ is a piecewise linear function known as the check function.

3. Problem Formulation

This section defines the SOH assessment problem with a distributional output to enhance the model reliability. The SOH of a LIB is defined as follows [33].

$$SOH = \frac{Z_{max}^l}{Z_0} \times 100\% \tag{5}$$

where Z_{max}^l indicates the maximum capacity at l-th cycle. C_0 represents the initial capacity at the beginning of its service life. It is typically provided by the manufacturer and serves as a reference point. The SOH is

typically expressed as a percentage, where 100% represents the battery's initial capacity and performance when it was new.

Multiple sources of monitoring data, including current, voltage and temperature, can be used as the input for model construction. The objective of this work is to construct a projection from the monitoring data to the SOH percentage, which can be expressed as

$$SOH = f\left(X^l|\theta\right) \tag{6}$$

where f represents the project function. It maps the monitoring data X^l to the SOH assessment result by the function f parameterized by θ. X^l denotes the single source or multiple sources of monitoring data to reflect the health state of LIB. In this research, SOH result follows a specific distribution.

$$SOH^l := \mathbb{E}\left[Z\left(X\right)\right] = \mathbb{E}\left[F\left(X|\theta\right)\right] \tag{7}$$

This equation indicates distribution Z can also be represented by a cumulative distribution function F parameterized by θ. Traditionally, SOH is a value which could not be robust and ignores the uncertainty included in the process of cycling and measurement. This work enhances the reliability of the SOH assessment result with a distributional output. In addition, this work optimizes the loss function to complete the trustworthy model training.

4. Methodology

4.1. General Procedure

This section introduces the general procedures of the proposed method, which is illustrated in Fig.2. It consists of three modules, namely data pre-processing, model training, model test as well as model evaluation and feature visualization. The details are described as follows.

1. Data collection and pre-processing. Multi-source data are collected from charging process of a LIB. The maximum capacity of LIB at each cycle can be calculated by the integral of current. This is used to construct the labels for model training and validation. Then the reference of SOH distribution is constructed according to the capacity label.
2. Model construction. Partial monitoring data as well as their labels are selected as training data to train the SOH assessment model. Deep features are extracted by Residual Networks (ResNet) and obtain the estimated SOH distribution over selected quantiles. This result enhances the reliability of SOH assessment.
3. Model training. The parameters of the network and predictor are optimized by a Wasserstein distance-based loss function to obtain a well-trained SOH assessment model. This loss function is calculated from the predicted SOH quantile distribution and the benchmark SOH quantile distribution.
4. Model test. The well-trained models are tested on the test data. The outcomes of the model are compared with the reference SOH to complete the evaluation of model performance.
5. Model evaluation and feature visualization. Multiple metrics are selected to evaluate the goodness of fit of SOH quantile distributions the estimation error of SOH values. The extracted features from ResNet are visualized to analyze the feature performance and enhance the interpretability of the network.

4.2. Residual Network

ResNets are employed to extract deep features from multi-source monitoring data. ResNet is a type of deep neural network architecture designed to address the issue of training deep neural networks. It was introduced by He et al. [34]. ResNet architectures are designed to effectively train very deep neural networks. In the context of assessing SOH, the LIB's health status may depend on intricate patterns and features that require a deep understanding of the data. ResNet's ability to handle deep networks makes it suitable for capturing complex relationships within the battery data. The deep feature can capture high-level information. However, the provided dataset could feature small sample of data. Training a deep network on small sample data to obtain very deep features is easy to cause overfitting and fail to convergence. The introduction of residual connections in ResNet is a key innovation. These connections allow the model to learn residual information, making it easier

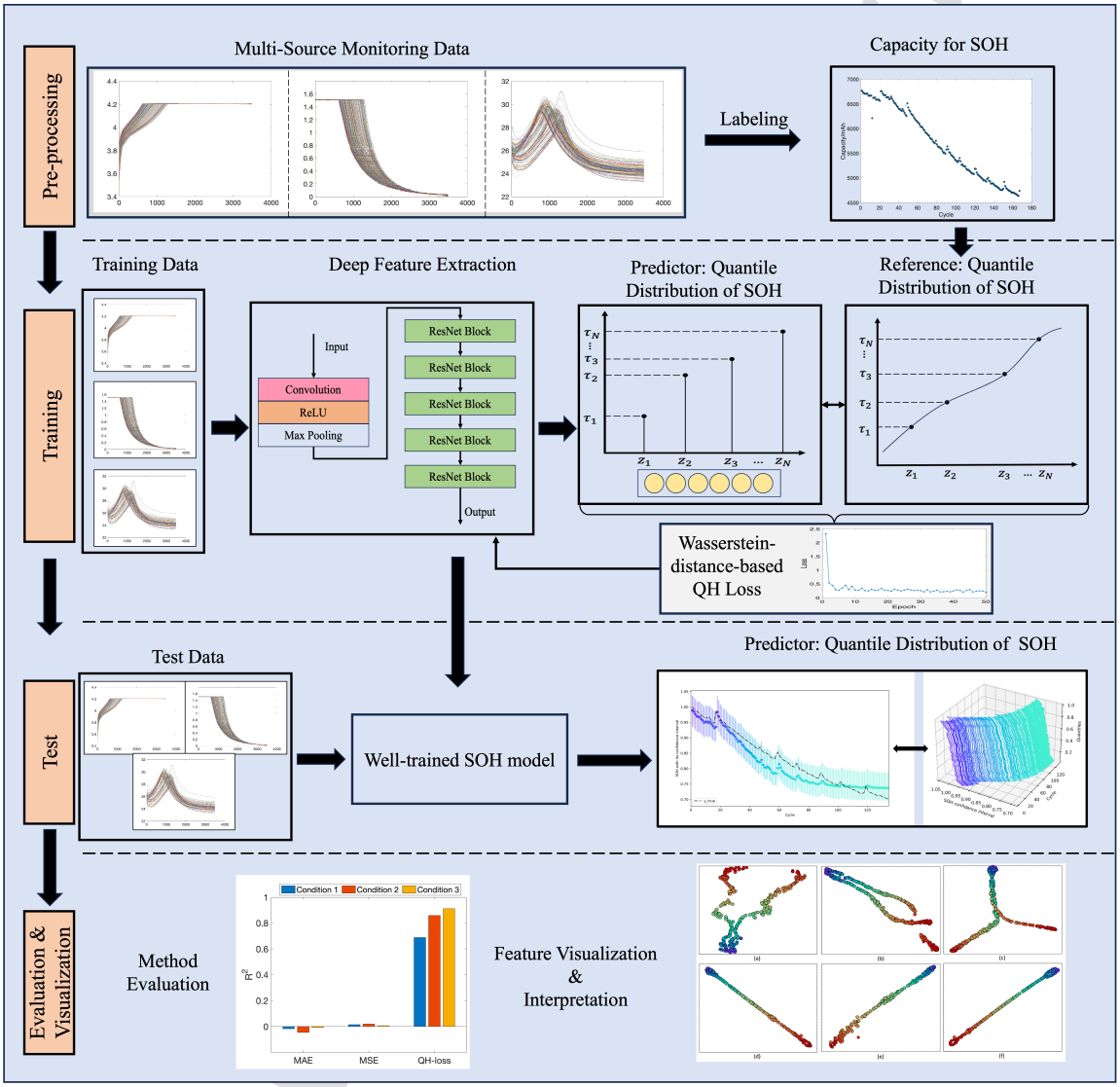

Figure 2: Framework of the proposed method. It consists of four steps, namely data pre-processing, ResNet model training, model test and model evaluation and feature visualization.

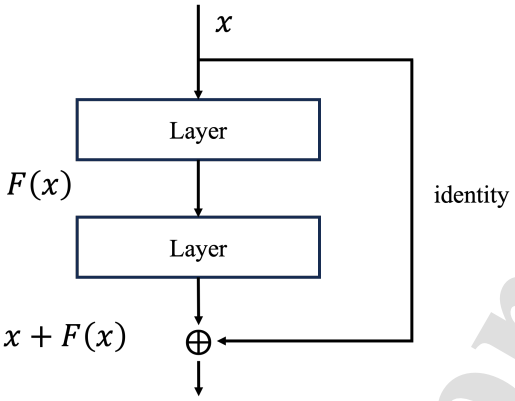

Figure 3: An example of residual block structure. It is composed of the identity path and the residual path. The output of the block summarizes the output of identity and residual paths.

to train deep networks. In the context of SOH assessment, where subtle changes in LIB behavior over time are crucial, these connections help capture and retain important information that might be lost in shallower architectures. In addition, LIB monitoring data often have temporal dependencies, and the health status may be influenced by how certain patterns evolve over time. ResNet's architecture, with its residual connections, is well-suited to capture and model temporal dependencies.

The innovative design of ResNet involves the use of residual blocks. It contains skip connections or shortcuts that allow the network to skip one or more layers. This design can mitigate the vanishing gradient problem that often occurs in deep networks. Residual blocks are the basic building block of a ResNet. A residual block consists of two main paths: the identity path and the residual path. The identity path simply passes the input through, while the residual path utilizes a set of computations to the input. The output of the block summarizes the output of identity and residual paths. Fig.3 illustrates a structure of the residual block. In the example, the residual connection skips two layers.

Suppose that the output of the l-th residual block is the input to the $(l+1)$-th residual block, then the network obtains the following result [35].

$$x^{(l+1)} = F(x^{(l)}) + x^{(l)} \tag{8}$$

In the block,

$$F(x) = W_2\sigma(BN(W_1\sigma(BN(x)) + b_1)) + b_2 \tag{9}$$

where BN represents the batch normalization operation. The term $W_1\sigma(BN(x)) + b_1$ represents the output of the first convolutional layer, and the subsequent operations are similar to the structure. With this block conducted recursively, the output can be expressed by

$$x^{(L)} = \sum_{i=1}^{L-1} F(x^{(i)})) + x^{(l)} \tag{10}$$

Residual learning offers an additional advantage by partially mitigating the vanishing gradient problem. Nevertheless, it is important to recognize that the degradation issue is not solely attributable to the vanishing gradient problem, as normalization layers have already been employed to address it. By differentiating with

respect to $x^{(l)}$ based on the aforementioned forward propagation, the derivation is obtained [36]

$$\begin{aligned}\frac{\partial \mathcal{L}}{\partial x^{(l)}} &= \frac{\partial \mathcal{L}}{\partial x^{(L)}} \frac{\partial x^{(L)}}{\partial x^{(l)}} \\ &= \frac{\partial \mathcal{L}}{\partial x^{(L)}} \left(1 + \frac{\partial \sum_{i=1}^{L-1} \left(F(x^{(i)})\right)}{\partial x^{(l)}}\right) \\ &= \frac{\partial \mathcal{L}}{\partial x^{(L)}} + \frac{\partial \mathcal{L}}{\partial x^{(L)}} \frac{\partial \sum_{i=1}^{L-1} \left(F(x^{(i)})\right)}{\partial x^{(l)}}\end{aligned} \tag{11}$$

where $\mathcal{L}$ is the loss function to be selected for parameter optimization. This expression implies that when computing the gradient of a shallow layer $\frac{\partial \mathcal{L}}{\partial x^{(l)}}$, there consistently exists a component $\frac{\partial \mathcal{L}}{\partial x^{(L)}}$ directly incorporated. It can effectively avoid the gradient vanishing problem even if the gradient of $F(x^{(i)})$ is small.

4.3. Reliable SOH Assessment

The proposed method predicts the quantiles of the SOH value distribution Z. The discrete SOH values derived from CDF of Z are $\tau_1, \cdots, \tau_N$, where $\tau_i = 1/N$, for $i = 1, \cdots, N$. Then the SOH quantile distribution $Z_\theta \in Z$ maps the observation x to a distribution parameterized by $\theta_i(x)$, which is given by

$$Z_\theta(x) := \sum_{i=1}^{N} \delta_{\theta_i(x)} \tag{12}$$

where δ represents the Dirac delta function. In this work, the Wasserstein metric-based method is proposed for model optimization and a quantile regression [37] implements the SOH distribution prediction.

4.4. Wasserstein Distance-based QH loss

To complete the optimization with a quantile regression result, a novel Wasserstein distance-based QH loss is proposed and constructed based on the quantile regression loss and typical Huber loss. The Huber loss is expressed by [38]

$$L_\kappa(u) = \begin{cases} \frac{1}{2}u^2 & , if\ |u| \leqslant \kappa \\ \kappa\left(|u| - \frac{1}{2}\kappa\right) & , \text{otherwise} \end{cases} \tag{13}$$

The quantile regression loss is define as

$$L_{QR}^{\tau} := \mathbb{E}_{\hat{Z} \sim Z}\left[\rho_\tau\left(\hat{Z} - Z\right)\right] \tag{14}$$

where

$$\rho_\tau(u) = u\left(\tau - \delta_{\{u<0\}}\right), \forall u \in \mathbb{R} \tag{15}$$

$Z : \{z_1, z_2, \cdots, z_n\}$ means the value of quantile function $F_Z^{-1}(\tau)$, $\tau \in [0, 1]$. The combination of the two losses derives [39]

$$\rho_\tau^\kappa(u) = |\tau - \delta_{u<0}| L_\kappa(u) \tag{16}$$

Due to the ground-truth label of capacity y is a distribution function rather than a value in the quantile Huber loss. Consequently, a CDF of target distribution $F_Z(y)$ is designed with the capacity label y. The CDF is assumed to follow the Gaussian distribution function, which is denoted as follows.

$$F_Z(y) = \frac{1}{\sigma\sqrt{2\pi}} \int_{-\infty}^{y} \exp\left(-\frac{(\tau - \mu)^2}{2\sigma^2}\right) \mathrm{d}t \tag{17}$$

In terms of the above derivation and Wasserstein distance, a novel loss is proposed for the proposed method. The Wasserstein distance-based QH loss is expressed as

$$L_W = \sum_{i=1}^{N} \mathbb{E}\left[\rho_{\hat{\tau}_i}^\kappa\left(F_Z^{-1}(\hat{\tau}_i) - G_P(\hat{\tau}_i | G_F(x))\right)\right] \tag{18}$$

where G_F and G_P represent the function of deep feature extraction and the capacity distribution predictor, and then $G_P(\hat{\tau}_i | G_F(x))$ indicates the predicted quantile distribution at every quantile $\hat{\tau}_i$. By minimizing the above loss function, the optimal parameters of deep network and quantile regression for SOH evaluation can be achieved.

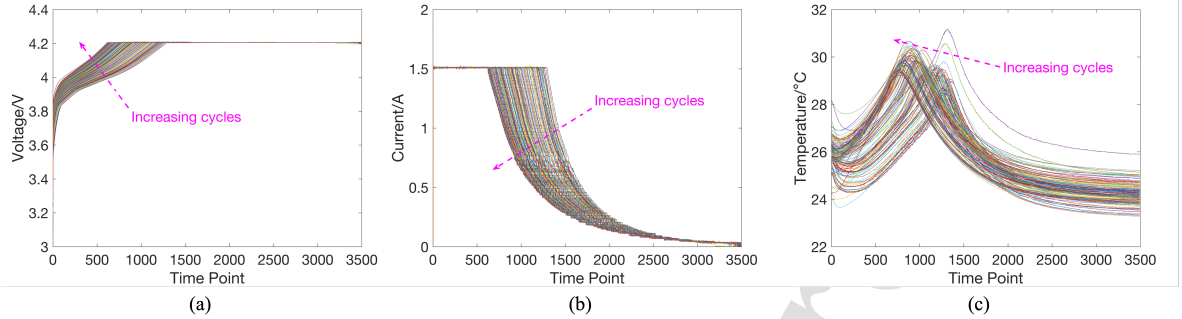

Figure 4: Monitoring data over cycles (a)Voltage (b)Current (c) Temperature. These figures showcase the variations of voltage, current and temperature signals over cycles during charging.

5. Experimental Validation

5.1. Data Description

Three lithium-ion batteries (referred to as #5, #6, and #7) from the NASA data set [25] were employed to validate the proposed method. These batteries were subjected to three distinct operational profiles (charge, discharge, and impedance) while maintained at room temperature. The charging process for these batteries followed a constant current-constant voltage (CC-CV) mode. Charging commenced in a constant current (CC) mode at a rate of 1.5A until the battery voltage reached 4.2V. It then transitioned to a constant voltage (CV) mode until the charge current decreased to 20mA. Discharging, on the other hand, was carried out at a constant current (CC) of 2A until the battery voltage reached 2.7V, 2.5V, and 2.2V for batteries 5, 6, and 7, respectively. The aging of these batteries was accelerated through repeated cycles of charging and discharging. The experiments were terminated when the batteries met the end-of-life criteria, which was defined as a 30% reduction in their rated capacity. Fig. 4 (a)-(c) display the voltage, current, and temperature data for battery #5 throughout the entire charging cycles.

5.2. SOH Assessment

The three LIBs are used to validate the proposed method. The experiments were conducted on a computer equipped with a single Nvidia GeForce GTX 2060 GPU, an Intel Core i7-10750H CPU running at 2.60 GHz, and 16 GB of memory. After the data are pre-processed, they are split into training data and test data. The detailed information for the split is shown in Tab. 1. In the three conditions, two LIB datasets are used to train a model and the rest one is used to test the model.

Table 1: Experimental Data Split

Condition	Training Data	Test Data
1	6# battery 7# battery	5# battery
2	5# battery 7# battery	6# battery
3	5# battery 6# battery	7# battery

These data are first input into a ResNet model to extract deep features. The designed structure of ResNet and feature extractor are given in Tab.2. In the table, the feature extractor gives the overall frame of the designed ResNet for SOH assessment. It consists of 4 ResNet blocks, each of which consists of a base layer, a match layer and a shortcut connection layer. The output of the ResNet is input into a predictor to give a reliable result of SOH distribution. The parameter settings of the proposed method are summarized in Tab.3. They are optimized with the proposed Wasserstein Distance-based QH loss.

Table 2: Feature Mapping Structure of ResNet

	Block	Layer type	Kernel	Stride	Channels in	Channels out
Feature Extractor	1	Convolution	7×1	2×1	1	16
		ReLU				
		Max Pooling	3×1	2×1		
	2	ResNet Block			16	32
	3	ResNet Block			32	64
	4	ResNet Block			64	64
	5	ResNet Block			64	64
ResNet Block	Base layer	Convolution	3×1	1×1	N_{in}	N_{out}
		BatchNorm				
		ReLU				
		Convolution	3×1	1×1	N_{out}	N_{out}
		BatchNorm				
	Match Layer	Convolution	1×1	1×1	N_{in}	N_{out}
		BatchNorm				
	Shortcut Connections	if $N_{in} = N_{out}$: $y = F(x, W_i) + x$				
		else: $y = F(x, W_i) + W_s x$				
		Where: W_i is Base Block and W_s is the Match Block				
		ReLU	$y = ReLU(y)$			

Table 3: Parameter setting of the proposed method

Parameters	Value
Learning rate	0.001
Batch size	32
Maximum epochs	500
N_τ	33
κ value	1.0
Target distribution factor σ	0.2

The outcomes of SOH assessment are demonstrated in Fig.5(a)(c)(e), where the black dotted line and the color line indicate the ground truth of SOH and the predicted SOH distribution; each color line represents the SOH distribution at the corresponding cycle; the dots on the color lines represent the medium of SOH value; the color changes from the blue to green, indicating the SOH degradation degree of LIB varies from the normal condition to the failure condition. Figs.5(b)(d)(f) show the 3-D visualization of the cumulative distribution of evaluated SOH at each cycle. The three axes indicate cycle number, quantiles and SOH values, respectively. They show the estimated SOH across cycles and quantiles. These figures reveal a noteworthy consistency between the predicted results and the actual SOH values. Furthermore, it can be seen that the confidence interval includes a range of value around the median SOH. These estimated distributions considered the uncertainty that occurred during data collection or modeling. The visual representation of SOH distribution in the proposed method demonstrates the model can not only assess the SOH values of LIB but also capture uncertainty at each cycle, which enhances the reliability of the proposed method and the SOH results. The optimized model exhibits precise outcomes of SOH, successfully learning the LIB degradation patterns from training data.

However, the uncertainty presents different variations in different results. For 5# LIB and 6#LIB, the uncertainty does not present obvious variation. This means the system remains stable over cycles. By contrast, 7#LIB presents a decreasing trend. This may be caused by the random events or absence of knowledge for model construction. In Figs.5(c), the performance of 6#battery appears to be suboptimal. One potential explanation for this observation could be the significant difference in the degradation pattern of the LIB compared to 5# and 7# LIBs. In the case of condition 2, the model was trained on data from 5# and 7#LIBs but tested on data of 6#LIB . Despite the enhanced generalization ability of the proposed method, it exhibits a certain limitation in handling distinct degradation patterns. In contrast, the degradation patterns of 5#LIB and 7#LIB may exhibit similarity, leading to better performance when the model is trained on mixed data from LIB 5 and tested on LIB 7 or vice versa.

In addition, one phenomenon that cannot be neglected is that the distributions exist estimated SOH values that exceed one, especially in the initial cycles. In many cases, SOH values are normalized for easy interpretation, with 1 representing the optimal or healthy state. This normalization allows for a standardized scale across different systems. However, our model gives the SOH distribution as the evaluation result. In a distribution context, normalization to a strict range may not be applicable for every individual data point. The distribution may naturally extend beyond this range, reflecting the variability in the health states of different elements within the system. Especially in the intial cycles, the SOH values tend to be quite close to one, and the SOH distribution gives the maximum probability at one (or close to 1). To give a complete distribution, it is avoidable that values that exceed 1 exist. This is one possible explanation. On the other hand, values exceeding one do not necessarily indicate an error or anomaly. Instead, they represent instances where certain components or elements in the system may be healthier than the intial state.

5.3. Analysis of Convergence Ability

Fig.6 illustrates the convergence of the Wasserstein distance-based QH loss for optimization throughout the training process on the three LIBs. From these figures, it is evident that the proposed loss function can converge successfully. This visualization underscores the effectiveness of the new Wasserstein distance-based QH loss in convergence.

5.4. Method Comparison

Three metrics are adopted in the section to evaluate the performance of the proposed method for the SoH of LIBs quantitively, which consists of the mean absolute error (MAE), the root mean square error (RMSE) and the R^2 score.

The MAE measures the average absolute difference between the predicted and actual values. It is calculated by taking the mean of the absolute differences between each predicted and actual value.

The RMSE is similar to MAE but gives more weight to large errors. It is calculated by taking the square root of the average of the squared differences between the predicted and actual values.

The R^2 score, also known as the coefficient of determination, is a statistical metric used to evaluate the goodness of fit of a regression model. The R^2 score ranges from 0 to 1, where 0 indicates that the model does

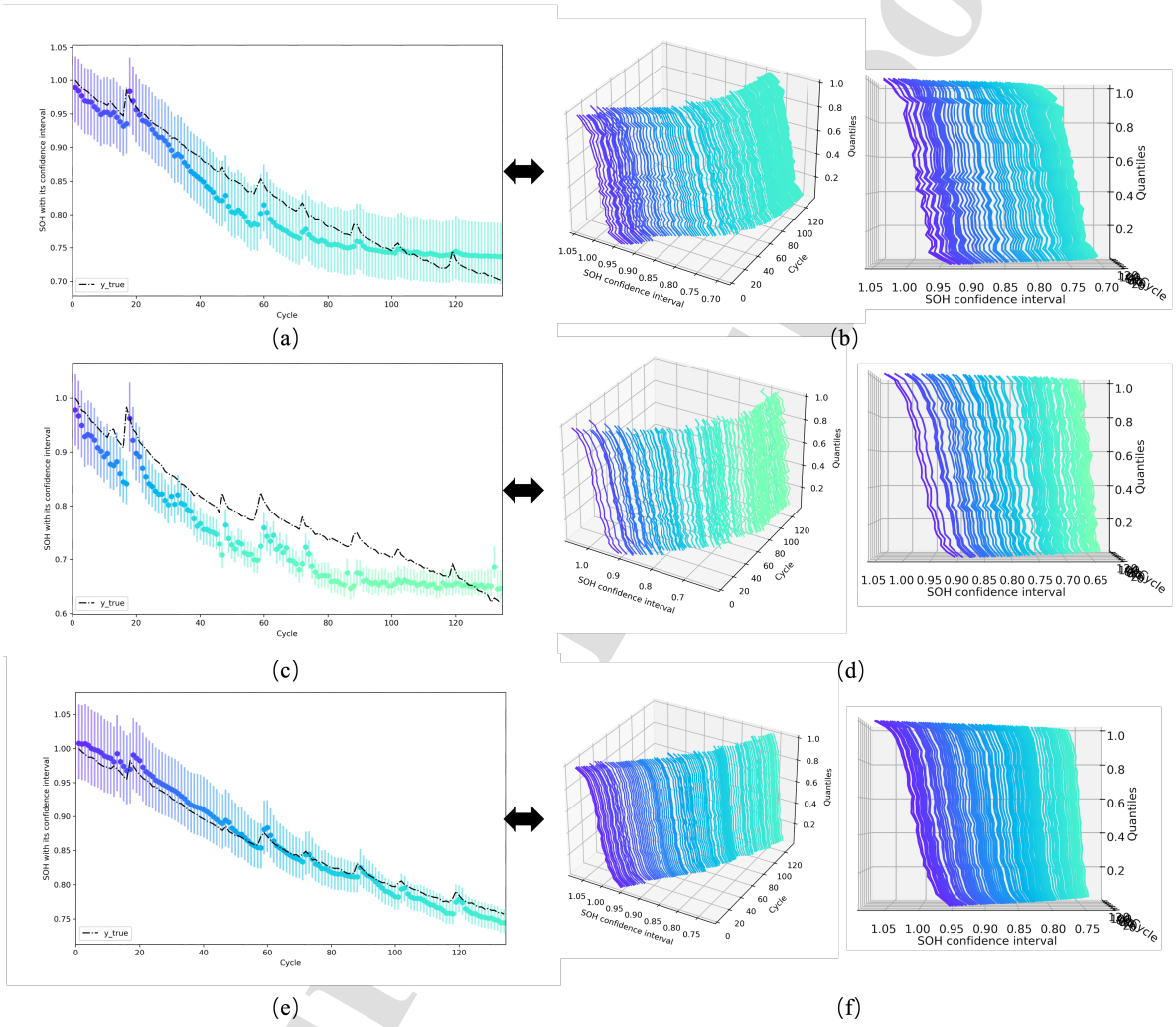

Figure 5: The SOH assessment.(a) The ground-truth and predicted SOH result of 5#LIB (b) Multi-view 3-D visualization of SOH distribution of 5#LIB (c) The ground-truth and predicted SOH result of 6#LIB (d) Multi-view 3-D visualization of SOH distribution of 6#LIB.(e) The ground-truth and predicted SOH result of 7#LIB (f) Multi-view 3-D visualization of SOH distribution of 7#LIB. The 2D view depicts the variation of the SOH distribution over cycles; the 3D view illustrates the coupled representation of the SOH distribution with confidence intervals across quantiles and cycles.

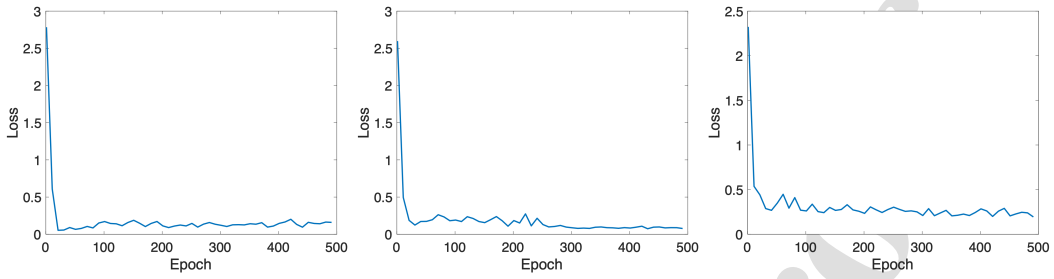

Figure 6: The convergence of model with Wasserstein distance-based QH loss. (a) convergence of 5#LIB (b) convergence of 6#LIB (c) convergence of 7#LIB. These figure gives the convergence process during training with the proposed loss, which proves its convergence ability.

not explain any of the variability in the target variable, and 1 indicates that the model perfectly fit to the target variable. These metrics are displayed as follows.

$$MAE = \frac{1}{K}\sum_{k=1}^{K}\left|\hat{C}_k - C_k\right| \tag{19}$$

$$RMSE = \sqrt{\frac{1}{K}\sum_{k=1}^{K}\left(\hat{C}_k - C_k\right)^2} \tag{20}$$

$$R^2 = 1 - \frac{\sum_{k=1}^{K}\left(\hat{C}_k - C_k\right)^2}{\sum_{k=1}^{K}\left(\bar{C}_k - C_k\right)^2} \tag{21}$$

where K is the total number of charge cycle. $\hat{C}_k$ is the predicted capacity, and C_k is the reference capacity.

5.4.1. Comparison with Other Loss Functions

The proposed Wasserstein distance-based QH loss is compared with the conventional MSE and MAE loss functions in this application.

The evaluation metric used for comparison is R^2, and the outcomes, depicted in Fig.7, clearly illustrate the superior performance of the proposed Wasserstein distance-based QH loss function over MSE and MAE when employing the same model structure. The network optimized with the proposed loss function achieves the highest R^2 score. This means that the predicted SOH distribution fits the true distribution with the highest precision when the network is optimized by the proposed loss.

5.4.2. Comparison with Other Deep Networks

To further demonstrate the superiority of the proposed method, three additional deep feature mapping structures (LSTM, CNN and DenseNet) are selected for comparison with the ResNet structure in the proposed method. The detailed structures of networks are summarized as follows.

The DenseNet has five blocks similar to CNN in the proposed method, but they are following the structure of DenseNet in reference [40].

The CNN consists of three convolutional blocks, each performing convolution, followed by a ReLU function for nonlinear transformation, and max pooling for downsampling. In the three blocks, the kernel sizes are 5×1, 3×1, and 3×1, respectively, with a pooling ratio set to 2 for all.

The LSTM structure follows the reference [41]. It consists of three LSTM units. The training process was conducted for 50 epochs by utilizing a learning rate scheduling. The initial learning rate of 0.01 was dropped with a factor of 0.2 after seven epochs.

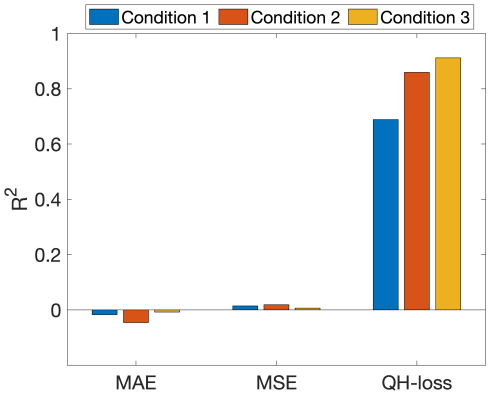

Figure 7: R^2 of the different loss functions. This figure demonstrates the discrepancies of SOH distribution calculated by the ResNet with MAE, MSE and the proposed QH loss for condition 1-3, respectively. The evaluation of these discrepancies is performed using the R^2.

The quantified results are presented in Table 4. By examining the MAE and RMSE, it becomes evident that the ResNet model attains the lowest error values. The predicted values exhibit the least deviation from the ground truth. In addition, the output of ResNet achieves the highest value of R^2 metric. This suggests that the output of ResNet consistently aligns with the ground-truth SOH distribution. Overall, the ResNet has achieved the best performance in comparison with CNN, LSTM and DenseNet. It can avoid the gradient vanishing problem and improve the efficiency of model training. Therefore, the ResNet structure is selected in the application to extract deep features for SOH prediction.

Table 4: Comparison with other deep neural network

Compared Network	Evaluation Metric	LIB Battery		
		5#	6#	7#
LSTM	MAE	0.0943	0.1551	0.1662
	RMSE	0.1032	0.1653	0.1768
	R2	0.8171	0.7245	0.7933
DenseNet	MAE	0.1788	0.1372	0.2310
	RMSE	0.1892	0.1483	0.3586
	R2	0.7881	0.7102	0.6541
CNN	MAE	0.1088	0.0985	0.1499
	RMSE	0.1254	0.1056	0.1587
	R2	0.7051	0.7192	0.6684
ResNet	MAE	0.0792	0.0806	0.0432
	RMSE	0.0885	0.0951	0.0506
	R2	0.8871	0.8596	0.9523

5.4.3. SOH Feature Visualization

To further assess the efficacy of the proposed method to implement SOH assessment of LIBs, the features extracted from the linear layer located before the output layer are selected for visualization. The *t-SNE* is utilized to condense these high-dimensional features into two-dimensional visual representations. The visualization can gain more insights to the SOH degradation pattern.

The test data of 3 batteries are selected for feature visualization. The visualization results are depicted in Fig. 8, where the color bar ranges from 0 (red) to 100 (blue), representing the normalized ground truth SOH with

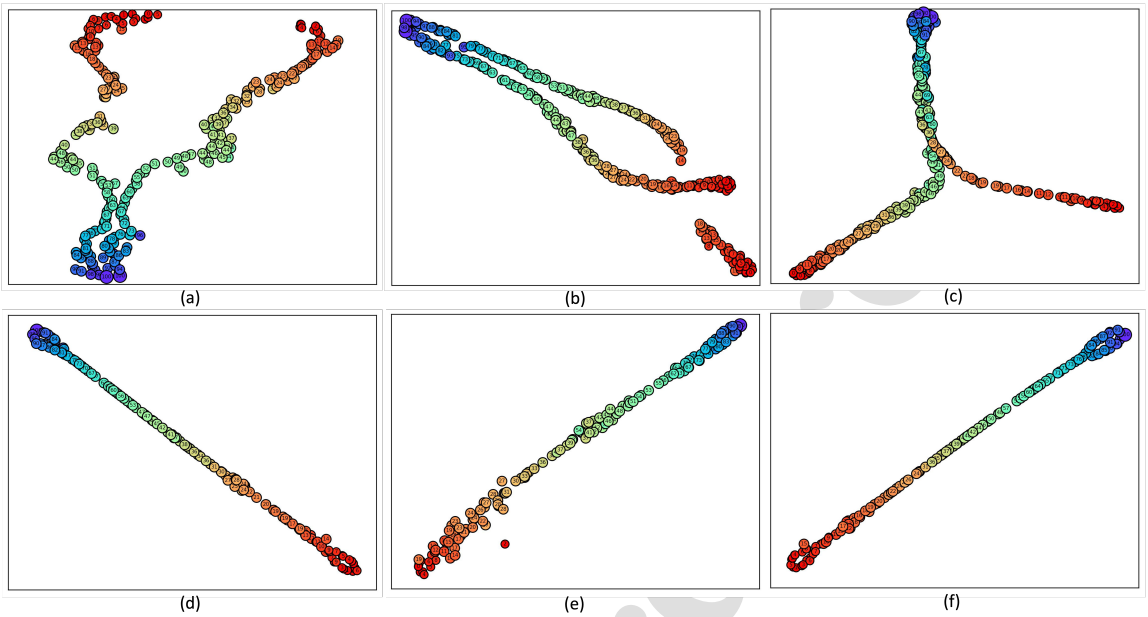

Figure 8: Feature Visualization. (a)Feature of training data of condition 1 (b)Feature of training data of condition 2 (c)Feature of training data of condition 3. These figures exhibit a regular transition of feature from 100 to 0 without evident mis-classification, which proves the effectiveness and generalization of the deep representation obtained from the well-trained network for LIB SOH.

a scaling factor of 100 applied for better visibility. The diverse feature visualization outcomes of the training data in condition 1-3 of Tab.1, as shown in Fig. 8(a), (b), (c), indicate well-trained models, as the labeled features exhibit a regular transition from 100 to 0 without evident mis-classification. The high generalization capability of the proposed method is confirmed by results from the unseen test data, presented in Fig.8(d), (e), (f). Despite the model not being exposed to the test data during training, it effectively recognizes varying degrees of SOH degradation.The proposed method captures the degradation pattern of LIB SOH effectively.

6. Conclusion and Discussion

This paper introduces a novel framework for SOH assessment based on deep learning. The proposed framework encompasses several key components, including the construction of a reference SOH distribution, model training with multi-source data, optimization using a Wasserstein distance-based QH loss, model test as well as model evaluation and feature visualization. This method enhances the precision of SOH estimation with comprehensive information.

A novel SOH assessment model, accounting for uncertainty, is introduced in this paper. The model constructs a quantile distribution of deep features, enabling the prediction of a SOH distribution with an associated confidence intervals. This approach enhances the reliability of SOH assessment and generalization ability of the SOH model. The quantile distribution is computed using deep features derived from the CNN. This strategy reduces reliance on domain expertise for the design of feature extraction schemes. Overall, the proposed approach not only considers uncertainty in SOH assessment but also leverages advanced loss functions and feature extraction methods, leading to a more reliable and generalized outcome.

A Wasserstein distance-based QH loss function is devised to implement the optimization of the proposed method. This loss function allows the proposed method to complete the optimization by quantifying the disparity between the estimated and ground truth of SOH distributions.

This proposed method is validated on the NASA dataset. The result demonstrates the effectiveness of the proposed method on enhancing the reliability of the SOH model. The visualization of the feature distribution shows the generalization ability of the model.

Though the proposed method achieves excellent performance in SOH assessment, a limitation of our proposed model is the presence of estimated SOH values exceeding one, particularly during the initial cycles. Addressing and optimizing this issue could be a focus for our future research.

Acknowledgements

This work is supported by National Natural Science Foundation of China (52275080).

References

[1] Y. Zhang and Y.-F. Li, "Prognostics and health management of lithium-ion battery using deep learning methods: A review," *Renewable and Sustainable Energy Reviews*, vol. 161, p. 112282, 2022.

[2] T. Han, J. Tian, C. Chung, and Y. M. Wei, "Challenges and opportunities for battery health estimation: Bridging laboratory research and real-world applications," *Journal of Energy Chemistry*, vol. 89, pp. 434–436, 2024.

[3] L. Zhang, T. Ji, S. Yu, and G. Liu, "Accurate prediction approach of soh for lithium-ion batteries based on lstm method," *Batteries*, vol. 9, no. 3, p. 177, 2023.

[4] C.-j. Wang, Y.-l. Zhu, F. Gao, X.-y. Bu, H.-s. Chen, T. Quan, Y.-b. Xu, and Q.-j. Jiao, "Internal short circuit and thermal runaway evolution mechanism of fresh and retired lithium-ion batteries with lifepo4 cathode during overcharge," *Applied Energy*, vol. 328, p. 120224, 2022.

[5] H. Meng and Y.-F. Li, "A review on prognostics and health management (phm) methods of lithium-ion batteries," *Renewable and Sustainable Energy Reviews*, vol. 116, p. 109405, 2019.

[6] X. Zhao, Z. Wang, E. Li, and H. Miao, "Investigation into impedance measurements for rapid capacity estimation of lithium-ion batteries in electric vehicles," *Journal of Dynamics, Monitoring and Diagnostics*, 2024.

[7] R. Xiong, Y. Zhang, J. Wang, H. He, S. Peng, and M. Pecht, "Lithium-ion battery health prognosis based on a real battery management system used in electric vehicles," *IEEE Transactions on Vehicular Technology*, vol. 68, no. 5, pp. 4110–4121, 2018.

[8] P. Kurzweil, W. Scheuerpflug, B. Frenzel, C. Schell, and J. Schottenbauer, "Differential capacity as a tool for soc and soh estimation of lithium ion batteries using charge/discharge curves, cyclic voltammetry, impedance spectroscopy, and heat events: A tutorial," *Energies*, vol. 15, no. 13, p. 4520, 2022.

[9] M. Messing, T. Shoa, and S. Habibi, "Estimating battery state of health using electrochemical impedance spectroscopy and the relaxation effect," *Journal of Energy Storage*, vol. 43, p. 103210, 2021.

[10] X. Sun, Y. Zhang, Y. Zhang, L. Wang, and K. Wang, "Summary of health-state estimation of lithium-ion batteries based on electrochemical impedance spectroscopy," *Energies*, vol. 16, no. 15, p. 5682, 2023.

[11] P. Vadhva, J. Hu, M. J. Johnson, R. Stocker, M. Braglia, D. J. Brett, and A. J. Rettie, "Electrochemical impedance spectroscopy for all-solid-state batteries: Theory, methods and future outlook," *ChemElectroChem*, vol. 8, no. 11, pp. 1930–1947, 2021.

[12] Y. Zhao, X. Yu, M. Chen, M. Zhang, Y. Chen, X. Niu, X. Sha, Z. Zhan, and W. J. Li, "Continuous monitoring of train parameters using iot sensor and edge computing," *IEEE Sensors Journal*, vol. 21, no. 14, pp. 15458–15468, 2020.

[13] N. Rangappa, Y. R. V. Prasad, and S. R. Dubey, "Lednet: Deep learning-based ground sensor data monitoring system," *IEEE Sensors Journal*, vol. 22, no. 1, pp. 842–850, 2021.

[14] H. Meng, M. Geng, and T. Han, "Long short-term memory network with bayesian optimization for health prognostics of lithium-ion batteries based on partial incremental capacity analysis," *Reliability Engineering & System Safety*, vol. 236, p. 109288, 2023.

[15] J. Wen, X. Chen, X. Li, and Y. Li, "Soh prediction of lithium battery based on ic curve feature and bp neural network," *Energy*, vol. 261, p. 125234, 2022.

[16] M. Cheng, X. Zhang, A. Ran, G. Wei, and H. Sun, "Optimal dispatch approach for second-life batteries considering degradation with online soh estimation," *Renewable and Sustainable Energy Reviews*, vol. 173, p. 113053, 2023.

[17] J. Jia, J. Liang, Y. Shi, J. Wen, X. Pang, and J. Zeng, "Soh and rul prediction of lithium-ion batteries based on gaussian process regression with indirect health indicators," *Energies*, vol. 13, no. 2, p. 375, 2020.

[18] K. Wu, J. Tan, and C. Liu, "Cross-domain few-shot learning approach for lithium-ion battery surface defects classification using an improved siamese network," *IEEE Sensors Journal*, vol. 22, no. 12, pp. 11847–11856, 2022.

[19] S. Han and Z. Feng, "Deep residual joint transfer strategy for cross-condition fault diagnosis of rolling bearings," *Journal of Dynamics, Monitoring and Diagnostics*, vol. 2, no. 1, pp. 51–60, 2023.

[20] S. Su, W. Li, J. Mou, A. Garg, L. Gao, and J. Liu, "A hybrid battery equivalent circuit model, deep learning, and transfer learning for battery state monitoring," *IEEE Transactions on Transportation Electrification*, vol. 9, no. 1, pp. 1113–1127, 2022.

[21] Y. Ma, C. Shan, J. Gao, and H. Chen, "Multiple health indicators fusion-based health prognostic for lithium-ion battery using transfer learning and hybrid deep learning method," *Reliability Engineering & System Safety*, vol. 229, p. 108818, 2023.

[22] H. Wang, Y.-F. Li, and Y. Zhang, "Bioinspired spiking spatiotemporal attention framework for lithium-ion batteries state-of-health estimation," *Renewable and Sustainable Energy Reviews*, vol. 188, p. 113728, 2023.

[23] J. Lu, R. Xiong, J. Tian, C. Wang, C.-W. Hsu, N.-T. Tsou, F. Sun, and J. Li, "Battery degradation prediction against uncertain future conditions with recurrent neural network enabled deep learning," *Energy Storage Materials*, vol. 50, pp. 139–151, 2022.

[24] Y. Chen, M. Rao, K. Feng, and G. Niu, "Modified varying index coefficient autoregression model for representation of the nonstationary vibration from a planetary gearbox," *IEEE Transactions on Instrumentation and Measurement*, vol. 72, pp. 1–12, 2023.

[25] B. Saha and K. Goebel, "Battery data set," *NASA AMES prognostics data repository*, 2007.

[26] W. Wang, Y. Lei, T. Yan, N. Li, and A. Nandi, "Residual convolution long short-term memory network for machines remaining useful life prediction and uncertainty quantification," *Journal of Dynamics, Monitoring and Diagnostics*, 2024.

[27] J. Zhang, Y. Jiang, X. Li, M. Huo, H. Luo, and S. Yin, "An adaptive remaining useful life prediction approach for single battery with unlabeled small sample data and parameter uncertainty," *Reliability Engineering & System Safety*, vol. 222, p. 108357, 2022.

[28] T. Zhou, T. Han, and E. L. Droguett, "Towards trustworthy machine fault diagnosis: A probabilistic bayesian deep learning framework," *Reliability Engineering & System Safety*, vol. 224, p. 108525, 2022.

[29] F. Wang, Z. Zhao, Z. Zhai, Z. Shang, R. Yan, and X. Chen, "Explainability-driven model improvement for soh estimation of lithium-ion battery," *Reliability Engineering & System Safety*, vol. 232, p. 109046, 2023.

[30] N. Tagasovska and D. Lopez-Paz, "Single-model uncertainties for deep learning," *Advances in Neural Information Processing Systems*, vol. 32, 2019.

[31] J. Zhang, P. Ma, W. Zhong, and C. Meng, "Projection-based techniques for high-dimensional optimal transport problems," *Wiley Interdisciplinary Reviews: Computational Statistics*, vol. 15, no. 2, p. e1587, 2023.

[32] J. Cui, Y. Xie, A. A. Joshi, K. Gong, K. Kim, Y.-D. Son, J.-H. Kim, R. Leahy, H. Liu, and Q. Li, "Pet denoising and uncertainty estimation based on nvae model using quantile regression loss," in *International Conference on Medical Image Computing and Computer-Assisted Intervention*, pp. 173–183, Springer, 2022.

[33] E. Chemali, P. J. Kollmeyer, M. Preindl, Y. Fahmy, and A. Emadi, "A convolutional neural network approach for estimation of li-ion battery state of health from charge profiles," *Energies*, vol. 15, no. 3, p. 1185, 2022.

[34] K. He, X. Zhang, S. Ren, and J. Sun, "Deep residual learning for image recognition," in *Proceedings of the IEEE conference on computer vision and pattern recognition*, pp. 770–778, 2016.

[35] M. Chang, D. Yao, and J. Yang, "Intelligent fault dignosis of rolling bearings using efficient and lightweight resnet networks based on an attention mechanism," *IEEE Sensors Journal*, 2023.

[36] H. Alaeddine and M. Jihene, "Deep residual network in network," *Computational Intelligence and Neuroscience*, vol. 2021, pp. 1–9, 2021.

[37] H. Zhang, Y. Su, F. Altaf, T. Wik, and S. Gros, "Interpretable battery cycle life range prediction using early cell degradation data," *IEEE Transactions on Transportation Electrification*, 2022.

[38] J. Cui, L. Yuan, L. He, W. Xiao, T. Ran, and J. Zhang, "Multi-input autonomous driving based on deep reinforcement learning with double bias experience replay," *IEEE Sensors Journal*, 2023.

[39] M. Zhang, D. Wang, N. Amaitik, and Y. Xu, "A distributional perspective on remaining useful life prediction with deep learning and quantile regression," *IEEE Open Journal of Instrumentation and Measurement*, vol. 1, pp. 1–13, 2022.

[40] G. Li, M. Zhang, J. Li, F. Lv, and G. Tong, "Efficient densely connected convolutional neural networks," *Pattern Recognition*, vol. 109, p. 107610, 2021.

[41] U. Yayan, A. T. Arslan, and H. Yucel, "A novel method for soh prediction of batteries based on stacked lstm with quick charge data," *Applied Artificial Intelligence*, vol. 35, no. 6, pp. 421–439, 2021.

Declaration of interests

☒ The authors declare that they have no known competing financial interests or personal relationships that could have appeared to influence the work reported in this paper.

☐The authors declare the following financial interests/personal relationships which may be considered as potential competing interests: